Experimental energy-band dispersions and magnetic exchange splitting for cobalt

F. J. Himpsel and D. E. Eastman
IBM Thomas J. Watson Research Center, Yorktown Heights, New York 10598
(Received 16 October 1979)

We have determined E vs $\vec{k}$ energy-band dispersions of cobalt for s and d bands along the hexagonal axis $\Gamma\Delta A$ ([0001] direction) via angle-resolved photoelectron spectroscopy from a Co(0001) face using synchrotron radiation. We obtain the magnetic exchange splitting at Γ for the upper d band (0.85 ± 0.2 eV) and lower d band (1.2 ± 0.3 eV). The overall occupied d-band width (~ 3.8 eV at L) is about 20% narrower than a state-of-the-art self-consistent band calculation using a local-density theory of exchange correlation. The top of the majority-spin d bands is 0.35 eV below E_F. There is a small Γ-centered minority-electron pocket at E_F which explains previously unidentified de Haas–van Alphen orbits. We present dipole selection rules for the Δ axis of an hcp lattice and show that the number of allowed transitions is reduced drastically for emission along the Δ axis. The allowed transitions can be interpreted in the same way as those for emission normal to a (111) face of an fcc lattice.

INTRODUCTION

Despite numerous band calculations[1-9] and photoemission studies,[10-15] the electronic structure of cobalt has not been determined accurately. Band-structure calculations[1-9] differ considerably concerning d-band width and ferromagnetic exchange splitting δE_{ex} e.g., δE_{ex} values from 0.8 to 4.3 eV have been reported. Photoemission experiments have been performed which give an overall picture of the density of states in Co.[10-15] A recent angle-resolved photoemission experiment[15] was unsuccessful in determining energy-band dispersions $E(\vec{k})$ because of the complexity of the exchange-split bands in an hcp lattice. An experimental estimate of $\delta E_{ex} \simeq 1.1$ eV has been obtained by comparing the maximum of the occupied d-band density of states obtained in ultraviolet photoemission spectroscopy (UPS) with calculations[12] and with the maximum of the empty d-band density states as obtained from x-ray continuum isochromats.[15,16] This value, which has a large uncertainty due to its method of determination, agrees with an estimate by Wohlfarth[17] based on magnetic and thermodynamic properties of cobalt.

Using angle-resolved photoemission combined with polarized tunable synchrotron radiation, we have successfully determined experimental energy-band dispersions $E(\vec{k})$ for the valence bands of ferromagnetic hcp cobalt along the line $\Gamma\Delta A$ in $\vec{k}$ space. We have obtained the magnetic exchange splitting at the Brillouin-zone-center Γ for both the upper d band Γ_{12} ($\delta E_{ex} = 0.85 \pm 0.02$ eV) as well as for the lower d band $\Gamma_{25'}$ ($\delta E_{ex} = 1.2 \pm 0.3$ eV). The top of the upper majority d band lies 0.35 eV below the Fermi level (this corresponds to the Stoner gap), and the bottom of the corresponding minority d band is 0.05 eV below E_F at Γ. This band topology gives rise to (at least) two electron pockets at Γ which explain experimental de Haas–van Alphen frequencies that theoretical studies have not identified previously.[18,7]

EXPERIMENTAL

For our measurements, a two-dimensional display-type electron spectrometer was used together with a 1.5-m toroidal grating monochromator and the 240-MeV storage-ring radiation source at the University of Wisconsin at Madison. This spectrometer, which permits angle-integrated and angle-resolved measurements, was operated with a full angular acceptance $\delta\theta = 5°$. The overall energy resolution of the system (electrons plus photons) was about 100 meV. For these conditions, count rates were typically 10^4/sec for the Co d bands for $h\nu \leq 25$ eV. A Co(0001) crystal surface was prepared by ion etching and annealing to ~350 °C with a working vacuum in the 10^{-11}-Torr range.

RESULTS

Selected normal-emission photoelectron-energy-distribution curves from a Co(0001) face are presented in Fig. 1 for different photon energies $h\nu$. These spectra sample the line $\Gamma\Delta A$ in $\vec{k}$ space because the momentum parallel to the surface is conserved. Data using s-polarized light ($\vec{E}$ vector in the surface plane) are shown in the left half of Fig. 1 while data for mixed sp polarization are shown in the right half. Because of dipole selection rules (to be discussed later), transitions from certain initial states cannot be seen in s polarization, e.g., from the sp band at $\simeq 1.5$ eV below E_F and from an sp-type Λ_1 surface state[19] at 0.3 eV below E_F. Surface-state emission is seen with p-polarized radiation and is given by the difference between the full-line curves (clean surface) and the dashed-line curves (surface contaminated with a

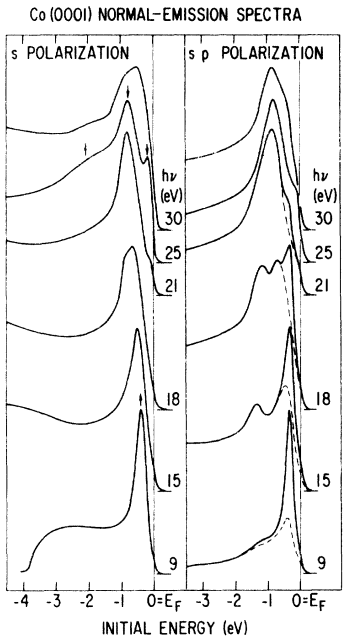

FIG. 1. Overview set of photoelectron spectra from Co (0001) showing the photon energy ($h\nu$) and polarization dependence for emission in the [0001] direction. Dashed lines are spectra with a submonolayer amount of hydrogen on the surface which suppresses emission from a Λ_1 surface state. In s polarization, the surface-state emission is symmetry forbidden. Arrows assign majority (↑) and minority (↓) d-band emission peaks.

submonolayer amount of hydrogen) in Fig. 1. The states seen using s-polarization are mostly d-like and their assignment to majority-spin-(up) and minority-spin-(down) states is shown in Fig. 1 for $h\nu = 9$ and 25 eV.

As we will show later, the spectra for $h\nu = 9$ and 25 eV sample states at the center (Γ) of the hcp Brillouin zone. The indicated majority-spin peak in the spectrum at $h\nu = 9$ eV (−0.35 eV) does not coincide with any of the peaks at $h\nu = 25$ eV (−0.05, −0.8, −2.0 eV). This results from the fact that the corresponding Γ states have different symmetries; these symmetries can be described in a simple way by comparing the hexagonal-close-packed (hcp) structure with a face-centered-cubic (fcc) close-packed structure having the same nearest-neighbor distance. The line $\Gamma\Delta A\Delta\Gamma$ in the hcp Brillouin zone (BZ) corresponds to the line $\Gamma\Lambda L$ in the fcc BZ [i.e., the direction perpendicular to the close-packed (111) face]. States at Γ in the hcp BZ correspond to states at Γ or L in the fcc BZ because of an extra lattice vector in the hcp lattice. The spectrum at $h\nu = 9$ eV samples states which are at the L point in the corresponding fcc BZ, while the spectrum at $h\nu = 25$ eV samples states which are at the Γ point of the corresponding fcc BZ. As we will show, dipole selection rules forbid transitions from an initial state of one kind of symmetry to final states of the other kind, i.e., from initial states at L to final states at Γ and vice versa in the corresponding fcc BZ. Therefore, transitions for normal emission from hcp Co(0001) can be classified in terms of an fcc Bz. In fact, the spectra are qualitatively very similar to normal emission spectra from Ni(111),[20] which has essentially the same nearest-neighbor distance.

Figure 2 gives an overview of the energy bands of Co along the [0001] direction using an fcc BZ diagram. Symmetry labels for both hcp and fcc BZ's are given. The initial states are taken from an *ab initio* ferromagnetic calculation for fcc cobalt[9]; the final states are for paramagnetic fcc cobalt using the same computational method[21] and have been shifted down by 1.5 eV to give an optimum fit to experimentally determined final-state critical points at Γ and L (marked by open circles). Symmetry assignments have been made for both hcp and fcc BZ's according to previous calcula-

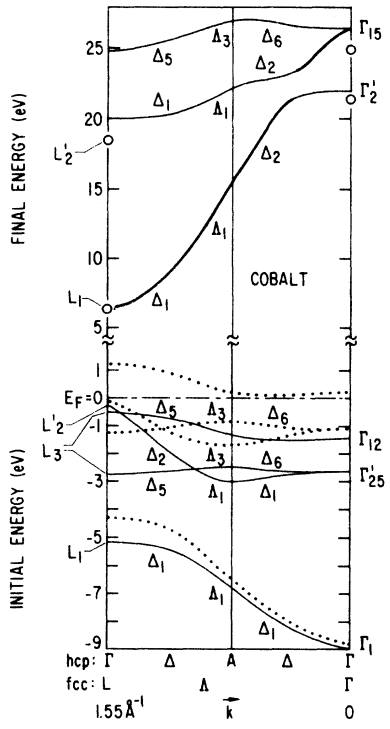

FIG. 2. Overview of the cobalt energy vs $\vec{k}$-band dispersions. Initial bands are from a ferromagnetic self-consistent calculation (Ref. 9) with majority-spin bands shown as full lines and minority-spin bands dotted. Final bands are from a similar paramagnetic calculation (Ref. 21) and have been shifted down by 1.5 eV to match our observed critical points (open circles). Symmetry assignments are given for both fcc and hcp lattices (see text). Only majority-spin bands are labeled for clarity.

tions[1-9] and a knowledge of the corresponding Ni bands.[20] Superimposing the bands shown in the left half [$\Gamma=(0,0,0,1)2\pi/c$ to A] and the right half [$\Gamma=(0,0,0,0)$ to A] of Fig. 2 by folding about A results in a complicated hcp-band structure which has hampered previous attempts to identify interband transitions.

Critical points of the final-state energy bands (open circles in Fig. 2) have been determined experimentally using extremal behavior of interband-transition intensities and peak positions, which habe been studied in detail for Ni and Pd for the corresponding fcc BZ.[20,22] For general points along the $\Gamma\Delta A$ line, we have used calculated final bands to interpolate[22] between the final-state critical points obtained directly and obtain $k_\perp$ from the observed final energy via the E-vs-$k_\perp$ dispersion of the final bands. This introduces only minor errors in $k_\perp$ ($\simeq 10\%$) and negligible errors for the initial energy ($\simeq 0.1$ eV) in the d-band region.

Using this analysis method, experimental energy dispersions $E(\vec{k})$ for the occupied $3d$ and $4s$ bands of ferromagnetic Co for the [0001] direction are shown in Fig. 3. The energy-to-$k_\perp$ conversion

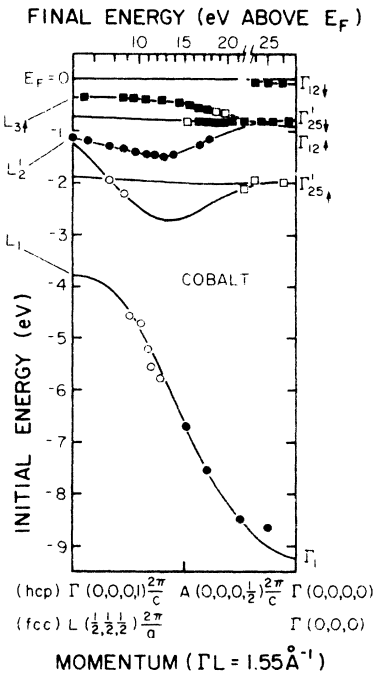

FIG. 3. Experimental E vs $\vec{k}$-band dispersions for cobalt using the final bands shown in Fig. 2 to determine the momentum $\vec{k}$ (see final energy scale on top of figure). Squares are bands with Λ_3 symmetry, circles are bands with Λ_1 symmetry (forbidden in s polarization). Open squares and circles are weak structures. The lines show the estimated topology of the energy bands.

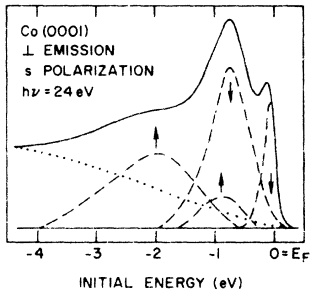

FIG. 4. Decomposition of a photoelectron spectrum from Co(0001) into transitions from two pairs of exchange-split Λ_3 bands (near the Γ point). For our analysis we assumed equal intensities for the lower strong pair of transitions and a secondary electron background (dotted curve). The position of the upper majority-spin transition is extrapolated from the results in Fig. 3.

scale is shown on top of the figure using the free-electron-like sections of the final bands (heavy lines in Fig. 2). We note that two exchange-split pairs of d bands with Λ_3 symmetry (fcc notation) are seen which are excited only by s-polarized radiation (squares in Fig. 2; the open squares are

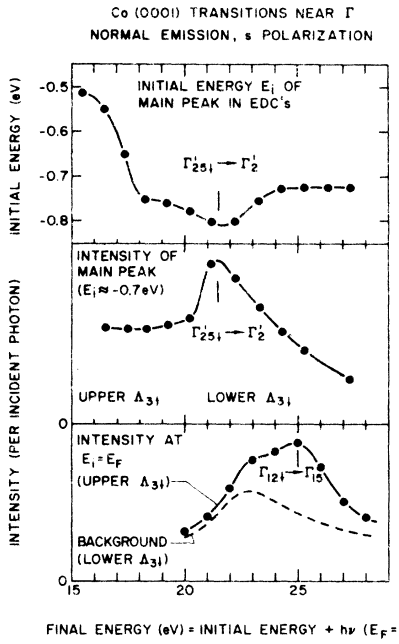

FIG. 5. Direct determination of critical points by observing extremal behaviors of transition intensities or peak energies with photon energy $h\nu$. The upper two panels show two independent determinations of the $\Gamma_{25}\downarrow$ and Γ_2' points. It is known from Pd(111) data (Ref. 22) that the lower Λ_3 band has a large matrix element for transitions into final states near Γ_2', whereas the upper Λ_3 band dominates for transitions into lower final states. The bottom panel monitors the intensity of transitions from the Γ-centered minority-spin electron pocket.

weak structures). They are associated with the Γ_{12} and Γ'_{25} critical points, respectively (fcc notation). With $h\nu$-dependent mixed sp-polarized radiation, one observes a pair of Λ_1-symmetry bands which connects from the L'_2 (sp-like) to the exchange-split Γ'_{25} critical points and one sees the lowest Λ_1-symmetry sp band between -4 and -9 eV (full and open circles in Fig. 3 with open circles being weak structures). The solid lines drawn through the data points in Fig. 3 show the topology of the bands as deduced from calculations (see Fig. 2). Some bands (e.g., the lower pair of Λ_3-symmetry bands near L) are not observed in our photon-energy range because of weak inter-band-transition matrix elements. This behavior has been observed for Cu, Ni, and Pd.[20,22-24] On the other hand, some transitions are known to dominate at certain photon energies (e.g., the lower pair of Λ_3-symmetry bands near the crossing of the first two final-state bands at $h\nu \sim 23$ eV). In this case, the lower partner of the exchange-split pair of bands appears weaker and washed out because of increased lifetime broadening. In the following we will discuss these intensity modulations in detail.

Upon taking account of different cross sections and an increasing Auger lifetime broadening for lower initial states, one can describe the photoelectron spectra accurately using the energy bands shown in Fig. 3. This is shown for a transition near the Γ point in Fig. 4. At this photon energy, the lower pair of exchange-split Λ_3 bands is much more intense than the upper pair. Upon lowering the photon energy, i.e., moving away from Γ towards L, the matrix element for the upper Λ_3 band starts to dominate ($h\nu \lesssim 19$ eV, see Fig. 1). The same effect is seen for Pd(111) normal emission data and has been used to determine critical points at Γ directly from experiment.[22] In general, points of higher symmetry in $\vec{k}$ space are expected to exhibit extremal behavior in inter-band transitions and intensities.[23]

In Fig. 5 selected inter-band-transition energies and intensities are plotted versus the final electron energy E_f (E_f equals initial energy plus photon energy). The final energy determines the momentum perpendicular to the surface, and consequently critical-point behavior should show up at certain final energies. In the upper panel, the initial energy position E_i of the main peak in the normal-emission photoelectron spectra (compare

TABLE I. Experimental and calculated energy values of critical points for cobalt (energies in eV with respect to the Fermi level).

Symmetry point fcc label (hcp label)	Experiment	Batallan *et al.*[a]	Moruzzi *et al.*[b]
$\Gamma_1\uparrow\downarrow$ ($\Gamma_1^+\uparrow\downarrow$)	-8.7 ± 1	-9.05	-8.90
$\Gamma'_{25}\uparrow$ $\begin{pmatrix}\Gamma_1^+\uparrow\\ \Gamma_6^-\uparrow\end{pmatrix}$	-2.0 ± 0.3	-2.27	-2.65
$\Gamma_{12}\uparrow$ ($\Gamma_6^+\uparrow$)	-0.9 ± 0.2	-1.46	-1.43
$\Gamma'_{25}\downarrow$ $\begin{pmatrix}\Gamma_1^+\downarrow\\ \Gamma_6^-\downarrow\end{pmatrix}$	-0.8 ± 0.1	-0.88	-1.14
$\Gamma_{12}\downarrow$ ($\Gamma_6^+\downarrow$)	-0.05 ± 0.05	-0.08	$+0.22$
$\Gamma'_2\uparrow\downarrow$	$+21.5 \pm 1$		
$\Gamma_{15}\uparrow\downarrow$	$+25.0 \pm 1$		
$L_1\uparrow\downarrow$ ($\Gamma_4^-\uparrow\downarrow$)	-3.8 ± 0.5	-4.55	-4.75
$L_3\uparrow$ ($\Gamma_5^+\uparrow$)	(-1.9 ± 0.4)	-1.89	-2.76
$L'_2\uparrow\downarrow$ ($\Gamma_3^+\uparrow\downarrow$)	-1.15 ± 0.2	-0.66	-0.23
$L_3\downarrow$ ($\Gamma_5^+\downarrow$)	-0.75 ± 0.2	-0.51	-1.28
$L_3\uparrow$ ($\Gamma_5^-\uparrow$)	-0.35 ± 0.05	-0.34	-0.53
$L_1\uparrow\downarrow$	$+6.4 \pm 0.5$		
$L'_2\uparrow\downarrow$	$+18.5 \pm 1.5$		

[a]Reference 7.
[b]Reference 9.

TABLE II. Experimental and calculated ferromagnetic exchange splitting δE_{ex} (values in eV averaged between splittings at Γ_{25}' and Γ_{12}).

	This experiment	Other experiments Ref. 11	Ref. 17	Ref. 18	Ref. 15
δE_{ex}	1.0	1.05	1.05	1.05[a]	1.05

	Calculations (*ab initio*) Ref. 2	Ref. 8	Ref. 9
δE_{ex}	2.0	4.3	1.6

	Calculations (semiempirical)[a] Ref. 1	Ref. 3	Ref. 4	Ref. 5	Ref. 6	Ref. 7
δE_{ex}	0.8	1.4	1.7	1.1	1.9	1.4

[a]Obtained from a paramagnetic calculation assuming a rigid splitting which is fitted to experimental data (e.g., the spin magnetic moment).

Fig. 1) is shown. There is a characteristic jump in E_i at about $E_f = 17$ eV which cannot be explained by an energy-band dispersion of the Λ_3 bands because they are dispersing slowly. Rather, the energy position E_i of the main peak is dominated by different initial bands below and above $E_f = 17$ eV with the upper $\Lambda_3\downarrow$ band dominating below $E_f = 17$ eV and the lower $\Lambda_3\downarrow$ band dominating above. The shallow minimum in E_i around $E_f = 21.5$ eV is attributed to the transition from the lower $\Lambda_3\downarrow$ band to the first final band at Γ ($\Gamma_{25}'\downarrow - \Gamma_2'$; i.e., $E_i = -0.8$ eV for $\Gamma_{25}'\downarrow$ and $E_f = 21.5$ eV for Γ_2'). This is confirmed by the intensity maximum of the main peak around $E_f = 21.5$ eV (middle panel of Fig. 5). The movement of the main peak in the range where the lower $\Lambda_3\downarrow$ band dominates can be attributed to the dispersion of this band from Γ to L, which would place the lower $L_3\downarrow$ point at -0.75 eV and the corresponding final state (L_2') at $E_f = 18.5$ eV. In the lowest panel, the intensity of the upper $\Lambda_3\downarrow$ band at $E_i = E_F$ is monitored. It is only visible in a narrow range of final energies [3.4 eV full width at half maximum (FWHM)] centered around $E_f = 25$ eV if one takes into account background from the tail of the lower $\Lambda_3\downarrow$ peak (see Fig. 4). Whereas the lower Λ_3 band couples mainly to the Γ_2' point, the upper Λ_3 band couples to the Γ_{15} point.[22] This gives $E_i = -0.05$ eV for the $\Gamma_{12}\downarrow$ point and $E_f = 25$ eV for Γ_{15}. In addition, we can estimate the size of the $\Gamma_{12}\downarrow$-centered minority-spin electron pocket. The half width of 1.7 eV for the upper $\Lambda_3\downarrow$ transition intensity vs E_f corresponds to a radius of $\approx 12\%$ of ΓL (i.e., 0.19 Å^{-1}) in $\vec{k}$ space (see final band dispersion in Figs. 2, 3).[25] With this radius, and the assumption of essentially a spherical pocket, one predicts that de Haas–van Alphen (dHvA) experiments should see orbits with areas of ≈ 0.03 a.u. This likely explains three

TABLE III. Dipole selection rules for the Λ axis ([111] direction) of an fcc lattice and for the corresponding Δ axis ([0001] direction) of an hcp lattice. p is the allowed transition for $\vec{E} \parallel \Lambda(\Delta)$ axis. s is the allowed transition for $\vec{E} \perp \Lambda(\Delta)$ axis.

(A) fcc lattice, [111] direction, symmetry group C_{3v}. For emission along the Λ axis the final state is Λ_1, i.e., only $\Lambda_1 \rightarrow \Lambda_1$ for $\vec{E} \parallel \Lambda$ axis, and $\Lambda_3 \rightarrow \Lambda_1$ for $\vec{E} \perp \Lambda$ axis are seen.

	Λ_1	Λ_2	Λ_3	Different notations
Λ_1	p		s	$\Lambda_1 = A_1$
Λ_2		p	s	$\Lambda_2 = A_2$
Λ_3	s	s	sp	$\Lambda_3 = E$

(B) hcp lattice [0001] direction, symmetry group C_{6v}. For emission along the Δ axis the final state is Δ_1 or Δ_2, i.e., only

$\Delta_1 \rightarrow \Delta_1$ for $\vec{E} \parallel \Delta$ axis,
$\Delta_2 \rightarrow \Delta_2$

and

$\Delta_6 \rightarrow \Delta_1$ for $E \perp \Delta$ axis are seen.
$\Delta_5 \rightarrow \Delta_2$

	Δ_1	Δ_2	Δ_3	Δ_4	Δ_5	Δ_6	Different notations
Δ_1	p					s	$\Delta_1 = A_1$
Δ_2		p			s		$\Delta_2 = B_1$
Δ_3			p			s	$\Delta_3 = A_2$
Δ_4				p	s		$\Delta_4 = B_2$
Δ_5		s		s	p	s	$\Delta_5 = E_2$
Δ_6	s		s		s	p	$\Delta_6 = E_1$

(C) Compatibility relations between C_{3v} and C_{6v} states via common symmetry operations

C_{3v}	Λ_1	Λ_1	Λ_2	Λ_2	Λ_3	Λ_3
C_{6v}	Δ_1	Δ_2	Δ_3	Δ_4	Δ_5	Δ_6

dHvA orbits that have been observed[18] ($\gamma = 0.033$ a.u., $\delta = 0.035$ a.u., $\eta = 0.037$ a.u.) but not theoretically predicted. These involve the minority-spin d band which is twofold degenerate and crosses the Fermi energy twice along ΓL near Γ (see calculated band topology[6] in Fig. 2 with E_F shifted up).

Table I summarizes the critical-point energies obtained directly from experiment using the extremal behavior of transitions near high-symmetry points. For comparison, we have included a recent *ab initio* ferromagnetic calculation for fcc cobalt (Ref. 9) and a calculation for hcp ferromagnetic cobalt using a rigid-band model with self-consistent nonmagnetic bands (Ref. 7).

For the magnetic exchange splitting δE_{ex} (averaged for the two fcc Γ points), we quote a larger sample of calculations in Table II. Gross discrepancies exist for δE_{ex}. Using the experimental spin magnetic moment μ, these discrepancies are difficult to resolve, e.g., two self-consistent calculations give $\mu = 1.58\mu_B$/atom, $\delta E_{ex} = 4.3$ eV (Ref. 8), and $\mu = 1.56\mu_B$/atom, $\delta E_{ex} = 1.5$ eV,[9] respectively, versus experimental values of $\mu = 1.56\mu_B$/atom, $\delta E_{ex} = 1.0$ eV at Γ. For a strong ferromagnet (i.e., filled majority d band and nearly empty minority d band) like cobalt, it turns out that the Fermi surface is mostly sp-like[7] and therefore reacts to the position of the d bands only via sp-d hybridization. This explains why Fermi-surface data are insensitive to δE_{ex}. Reducing δE_{ex} in the *ab initio* calculation of Ref. 9 to the observed value and readjusting the Fermi level properly results in a small Γ-centered electron pocket, as we observe.

This section describes group theoretical aspects of our comparison between the hcp and fcc lattices. Mainly it presents dipole selection rules which establish a one-to-one correspondence of hcp and fcc symmetry labels for emission along the threefold axis ([0001] for hcp and [111] for fcc). The symmetry groups are C_{6v} and C_{3v} for the hcp and fcc lattices, respectively. C_{3v} is a subgroup of C_{6v}. Therefore, each fcc state is related to two hcp states via the symmetry operations common to both groups (Table III C). The dipole selection rules and the restriction to final states which have nonvanishing wave functions in the direction of the threefold axis (Table III A, B as obtained from character tables using standard group-theory techniques, Refs. 26–28) select the following types of transitions: For the electric-field vector $\vec{E}$ perpendicular to the [0001] direction (s polarization) initial states of Δ_6, Δ_5 symmetry are excited into final states of Δ_1, Δ_2 symmetry, respectively. For $\vec{E}$ parallel to the [0001] direction we have the transitions $\Delta_1 \rightarrow \Delta_1$, $\Delta_2 \rightarrow \Delta_2$. Comparing calculated initial bands for hcp Co (Ref. 7) and fcc Co (Ref. 9) (see Fig. 2) we get qualitatively similar bands if we assign each Δ_1 (Δ_6) band to the half section of a Λ_1 band (Λ_3 band rsp.) which joins Γ. Likewise, the Δ_2 (Δ_5) bands correspond to the half sections of Λ_1 bands (Λ_3 bands rsp.) joining L. Using the same correspondence for the Δ_1, Δ_2 final bands, we obtain an fcc-type band structure with the proper fcc selection rules for allowed transitions in normal emission ([111] direction).

Notes added in proof. Recent calculations including self-energy corrections[29] predict that δE_{ex} should be larger for the t_{2g} (Γ_{25}')-type d bands than for the e_g (Γ_{12})-type d bands in nickel. This is what we find for cobalt. A calculation using local density exchange correlation[9] yields an opposite result for Co. Although the approximations made in Ref. 29 are not valid for Co, it would be interesting to pursue self-energy correction calculations.

The existence of a minority spin pocket near E_F is confirmed by recent measurements of spin-polarized photoemission[30] which exhibit negative spin polarization near the photothreshold.

ACKNOWLEDGMENTS

We wish to acknowledge A. Ignatiev for supplying the Co crystal and V. L. Moruzzi and A. R. Williams for providing calculated energy bands. We wish to thank J. J. Donelon, A. Marx, and the staff of the University of Wisconsin Synchrotron Radiation Center for their capable help. The storage ring is supported by the National Science Foundation under Contract No. DMR 77-21888. This work was supported in part by the Air Force Office of Scientific Research under Contract No. F44620-76-C-0041.

[1] L. Hodges and H. Ehrenreich, J. Appl. Phys. 39, 1280 (1968).
[2] J. D. Connolly, Int. J. Quantum Chem., Symp. 2, 257 (1968).
[3] K. C. Wong, E. P. Wohlfarth, and D. M. Hum, Phys. Lett. 29A, 452 (1969).
[4] S. Wakoh and J. Yamashita, J. Phys. Soc. Jpn. 28, 1151 (1970).
[5] Shoji Ishida, J. Phys. Soc. Jpn. 33, 369 (1972).
[6] R. A. Ballinger and C. A. W. Marshall, J. Phys. F 3, 735 (1973).
[7] F. Batallan, I. Rosenman, and C. B. Sommers, Phys. Rev. B 11, 545 (1975).
[8] C. M. Singal and T. P. Das, Phys. Rev. B 16, 5068 (1977).
[9] V. L. Moruzzi, J. F. Janak, and A. R. Williams, *Cal-*

culated Electronic Properties of Metals (Pergamon, New York, 1978).
[10]C. S. Fadley and D. A. Shirley, Phys. Rev. Lett. 21, 980 (1968).
[11]D. E. Eastman, J. Appl. Phys. 40, 1387 (1969).
[12]D. E. Eastman, J. Phys. (Paris), Colloq. C1, 293 (1971).
[13]S. Hüfner and G. K. Wertheim, Phys. Lett. 47A, 349 (1974).
[14]H. Höchst, S. Hüfner, and A. Goldmann, Phys. Lett. 57A, 265 (1976).
[15]P. Heimann, E. Marschall, H. Neddermeyer, M. Pessa, and H. F. Roloff, Phys. Rev. B 16, 2575 (1977).
[16]R. R. Turtle and R. J. Liefeld, Phys. Rev. B 8, 3411 (1973).
[17]E. P. Wohlfarth, J. Appl. Phys. 41, 1205 (1970).
[18]I. Rosenman and F. Batallan, Phys. Rev. B 5, 1340 (1972).
[19]F. J. Himpsel and D. E. Eastman, Phys. Rev. B 20, 3217 (1980).
[20]F. J. Himpsel, J. A. Knapp, and D. E. Eastman, Phys. Rev. B 19, 2919 (1979).
[21]V. L. Moruzzi and A. R. Williams (private communication).
[22]F. J. Himpsel and D. E. Eastman, Phys. Rev. B 18, 5236 (1978).
[23]E. Dietz and D. E. Eastman, Phys. Rev. Lett. 41, 1674 (1978).
[24]N. V. Smith, Phys. Rev. B 19, 5019 (1979).
[25]This value has an uncertainty of ~50% because the lifetime broadening of the final state is expected to be of the same magnitude as the observed width of the transition intensity vs E_f.
[26]W. Eberhardt and F. J. Himpsel (unpublished).
[27]C. Herring, J. Franklin Inst. 233, 525 (1942).
[28]J. F. Cornwell, Phys. Kondens. Mater. 4, 327 (1966).
[29]A. Liebsch, Phys. Rev. Lett. 43, 1431 (1979).
[30]M. Campagna (private communication).